PROCEEDINGS, 47th Workshop on Geothermal Reservoir Engineering
Stanford University, Stanford, California, February 7-9, 2022
SGP-TR-223

Seismoelectric Effects for Geothermal Resources Assessment and Monitoring: Overview and Preliminary Results

Christina Morency[1], Eric Matzel[1], Niels Grobbe[2], Daniel Brito[3], Clarisse Bordes[3], Natael Bernardo[3], Hélène Barucq[4], Julien Diaz[4], Arjeta Heta[4], Mathieu Bellanger[5], Mathieu Auxiètre[5], Kirsti Midttømme[6], Walter Wheeler[6], Roman Berenblyum[6], Bjarte Fagerås[7]

[1]Lawrence Livermore National Laboratory, CA, USA

[2]University of Hawai'i at Mānoa, HI, USA

[3]Université de Pau et des Pays de l'Adour, E2S UPPA, CNRS, Total, LFCR, Pau, France

[4]Inria, France

[5]TLS Geothermics, France

[6]NORCE Norwegian Research Center AS, Norway

[7]Monviro AS, Norway

E-mail: morency1@llnl.gov

Keywords: Seismoelectric Effects, Numerical Modeling, Laboratory Experiment, Field Experiment, Monitoring, GEOTHERMICA

ABSTRACT

Geothermal power plant operations circulate large amounts of fluid through the subsurface, but during the exploration phase, we typically have poor understanding of subsurface fluid transportation dynamics at reservoir depths. Being able to identify pre-existing water-filled fracture networks greatly helps to assess geothermal resources and targets. Mapping newly activated fracture networks can also help inform on and monitor stimulation successes and risk mitigation. Monitoring of geothermal resources rely predominantly on seismic techniques, which alone do not capture fluid-phase properties, while on the other hand, electromagnetic (EM) measurements add constraints to the fluid-phase properties, such as resistivity and permeability, but with little sensitivity to the rock structure. Here we are introducing the use of seismoelectric effects (SEE). These are pore-scale phenomena relying on electric charge separation created by streaming currents generated by pressure gradients, which occur when a seismic wave propagates. The SEE technique provides the benefits of both EM and seismic technologies, with estimated field survey costs that are similar to data acquisition of only a single data type, keeping operations affordable. This project relies on a fully integrated approach to assess the potential of SEE for the exploration and development of geothermal systems, based on numerical simulations, and experimental and field analysis. In the following, we validate the numerical implementation of SEE by showing agreement with the theory describing the existence of three types of SEE signals. We also show preliminary results for the laboratory and field experiments.

1. INTRODUCTION

The seismoelectric effects technique is a new and innovative approach for geothermal subsurface imaging and monitoring at reservoir scale. Our goal is to assess SEE in terms of data acquisition, cost and quality, and to determine its capability in comparison with classical imaging and monitoring techniques, particularly decoupled seismic and electromagnetic methods. Traditional seismic imaging techniques fail to resolve fluid-phase properties, while purely electromagnetic (EM) approaches typically provide limited, low-resolution constraints on the rock structure. Seismoelectric effects, pore-scale phenomena (Figure 1), arise from seismic-to-electromagnetic conversion in naturally charged porous media with a certain degree of fluid saturation.

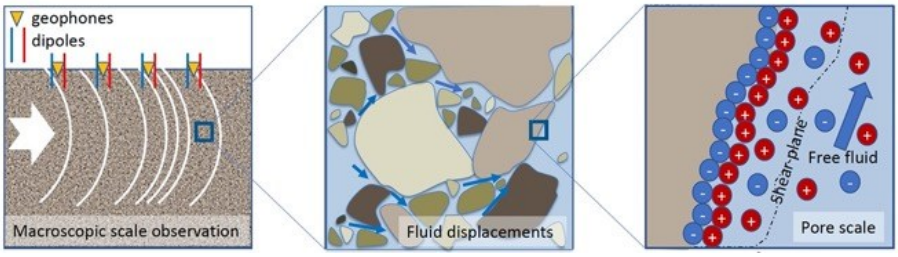

Figure 1: Schematic visualization of seismoelectric effects as pore scale electrokinetic phenomena.

As illustrated on Figure 2, in naturally charged, fluid-saturated, porous media, a propagating seismic wave causes pore-fluid flow through deformation of the rock and generates an electrical current. This electrical current induces an electromagnetic field, referred to as a

coseismic field, that propagates within the seismic wave. When this coseismic field is disrupted by subsurface heterogeneity (e.g., a contrast in mechanical or electrical properties), an electric dipole is created, triggering an independent EM field that is detectable in the far-field. This approach differs strongly from current state-of-the-art approaches that use joint, decoupled seismic-EM inversions, which integrate multiple data sets that were triggered and recorded separately. Those approaches increase the cost of field surveys and physically decouple the seismic and EM problems, which risks introducing physical errors due to strong nonlinear coupling, missing differentiating tight clay-filled fractures and pores from those containing water, and will potentially miss crucial phenomena such as the seismoelectric effects. The SEE technique, on the other hand, provides the benefits of both EM and seismic technologies, with estimated field survey costs that are similar to data acquisition of only a single data type.

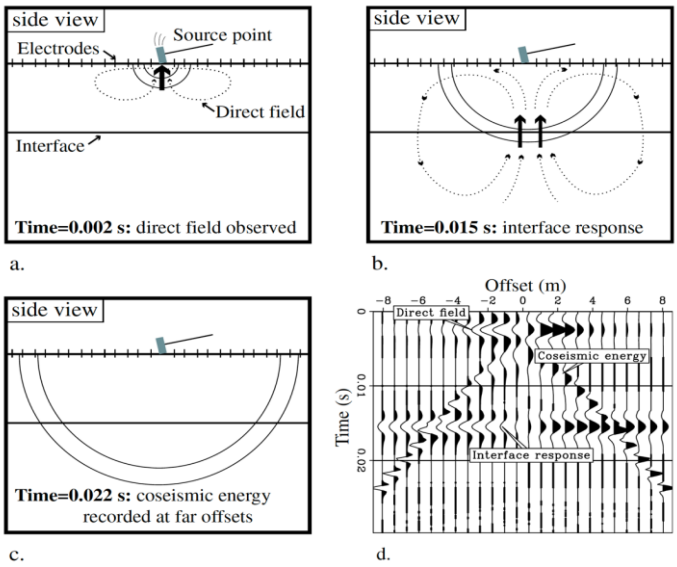

Figure 2: Schematic representation of seismoelectric survey and corresponding synthetic data. Panels (a), (b), and (c) show the propagation of the seismic wave. Note that in (c) the reflected seismic wave at the interface is neglected for simplicity. Corresponding SEE dataset, i.e., electric field, is plotted on panel (d), showing a direct field, interface response, and coseismic field (after Haines, 2004).

2. NUMERICAL MODELING

2.1 Theory

To model seismoelectric effects, we use similar governing equations as derived by Pride (1994), corresponding to Biot's poroelastic wave equations (Biot 1956a, 1956b) and Maxwell's electromagnetic wave equations coupled electrokinetically:

Biot seismic wave equations

$$\bar{\rho}\partial_t^2\mathbf{u}_s + \rho_f\partial_t^2\mathbf{w} = \nabla\cdot\mathbf{T} + \mathbf{f}$$
$$Y\partial_t\mathbf{w} + \rho_f\partial_t^2\mathbf{u}_s = \nabla\cdot\mathbf{T}_f + \mathbf{f} + \eta\mathbf{k}^{-1}L\mathbf{E}$$
$$\begin{cases} \mathbf{T} = (B\nabla\cdot\mathbf{u}_s + C\nabla\cdot\mathbf{w})\mathbf{I} + 2\mu_{fr}\mathbf{D}_s \\ \mathbf{T}_f = (C\nabla\cdot\mathbf{u}_s + M\nabla\cdot\mathbf{w})\mathbf{I} = -p_f\mathbf{I} \end{cases}$$

Maxwell EM wave equations

$$\nabla\times\mathbf{E} = -\partial_t\mathbf{B} - \mathbf{M}$$
$$\nabla\times\mathbf{H} = \partial_t\mathbf{D} + \mathbf{J} + \mathbf{C}$$
$$\mathbf{J} = L(\nabla\cdot\mathbf{T}_f - \rho_f\partial_t^2\mathbf{u}_s + \mathbf{f}) + \sigma\mathbf{E}$$
$$\begin{cases} \mathbf{D} = \epsilon\mathbf{E} \\ \mathbf{B} = \mu\mathbf{H} \end{cases}$$

$$Y \equiv \frac{\rho_f c}{\phi}\partial_t + \eta\mathbf{k}^{-1}$$

On the seismic side: $\mathbf{T}$ is the total stress, $\mathbf{T_f}$ and p_f are the fluid stress and pressure, respectively, μ_{fr} is the frame shear modulus, $\mathbf{f}$ is a macroscopic source, $\mathbf{u_s}$ the solid displacement, $\mathbf{w}$ the relative fluid displacement, $\mathbf{D_s}$ the solid strain deviator, ρ is the bulk density, ρ_f is the fluid density, η is the fluid viscosity, $\mathbf{k}$ is the fluid permeability. B, C, and M are Biot coefficients.

On the EM side: $\mathbf{H}$ and $\mathbf{E}$ are the magnetic and electric fields, respectively, $\mathbf{B}$ is the magnetic induction, $\mathbf{D}$ is the electric displacement, $\mathbf{M}$ and $\mathbf{J}$ are the magnetic and electric current density, respectively, ϵ is the dielectric permittivity, μ the magnetic permeability of the medium, σ is the electrical conductivity.

L is the electrokinetic coupling parameter.

We have developed two codes to solve these coupled equations, one using a spectral-element method (Morency and Tromp, 2008; Morency, 2020) in the time domain and one using a Discontinuous Galerkin technique in the frequency domain (Barucq et al., 2021).

2.2 SEE Modeling

Here we present preliminary SEE forward simulations performed using the spectral-element code for carbon storage monitoring to assess the numerical implementation. Figure 3 shows a schematic representation of our setup, which consists in a cross-well monitoring setup using a homogenous brined saturated porous medium. The seismic source is located in well A, and a series of collocated geophones and electrodes are in well B. Triggering the seismic sources leads to the propagation of a seismic wave and a coseismic electric signal. This coseismic field propagates at the same speed as the seismic field and is due to local fluid flow generated by the passage of the seismic wave (Figure 3).

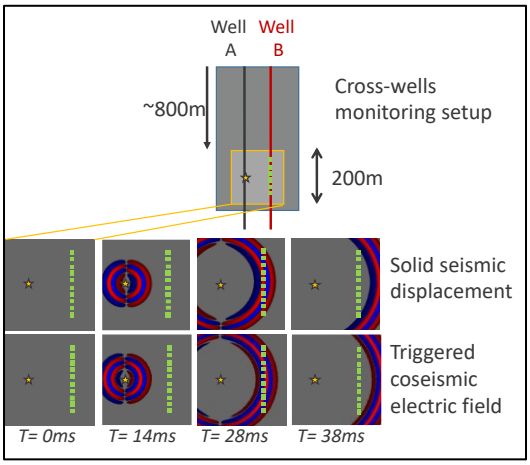

Figure 3: Geometry of the cross-well monitoring setup, and snapshots of the horizontal seismic displacement and coseismic electric field. The yellow star refers to the seismic source location and the green squares correspond to the collocations of the geophones and electrodes.

Next, Figure 4 (top) shows the corresponding vertical seismic displacement and electric field recorded at the collocated geophones and electrodes located in well B. We can see the compressional P-wave at the geophones. At the electrodes, in addition to the coseismic electric signal, we can also identify a quasi-instantaneous electric signal generated at the time when the seismic source is triggered, which is the so-called source-converted seismoelectric EM field. Then mimicking the intrusion of CO_2 in the initially homogeneous brine saturated porous medium, we trigger the seismic source and compare the recordings. Figure 4 (bottom) shows at the geophones a seismic P-wave, slightly delayed due to the change of properties between brine and CO_2 saturated porous media. The electric waveforms recorded at the electrodes not only show coseismic and source triggered electrical signals like in the previous case, but also display another, quasi-instantaneous seismoelectric conversion at the interface between the brine and the CO_2 saturation front.

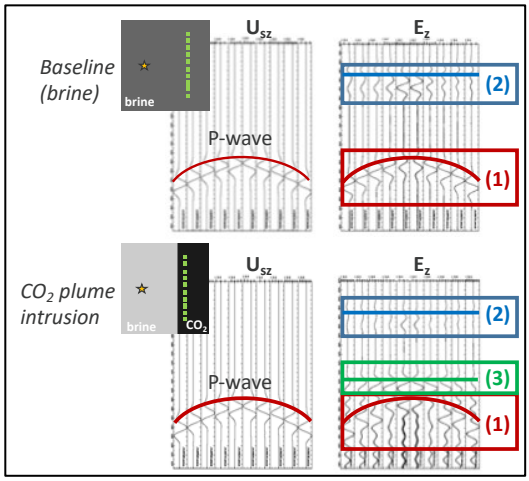

Figure 4: Vertical seismic and electric waveforms recorded at the collocated geophones and electrodes, respectively, after propagation in a homogeneous porous medium saturated with brine as baseline (top) and after intrusion of CO_2 (bottom). The recorded seismic signals correspond to the compressional P-wave. The recorded electric signals correspond to (1) coseismic electric signal, (2) quasi-instantaneous electric signal generated when the seismic source occurs, and (3) quasi-instantaneous interface response.

3. LABORATORY EXPERIMENTS

Using expertise of the past decades to characterize porous media properties effects on mechanical and EM wave propagation (e.g., Bordes et al., 2006, 2008; Holzhauer et al., 2015), we are designing new set of experiments to target SEE, which corresponds to a hybrid seismic-EM experiment compared to previous experiments. Using that setup (see Figure 5), we will be able to test the influence of physical parameters (temperature, salinity, permeability) on the SEE signal in the context of geothermal setting. These data will help validate our numerical methods and inform the optimal design of field surveys.

Preliminary results offer measurements of coseismic signals at electrodes buried in the sand (Figure 6) and measurements of seismic signals at the sand surface using a laser vibrometer (Shen et., 2022) (Figure 7). Comparing these two measurements leads to the transfer function E/u, which can be compared to Pride's theoretical prediction (see Figure 8).

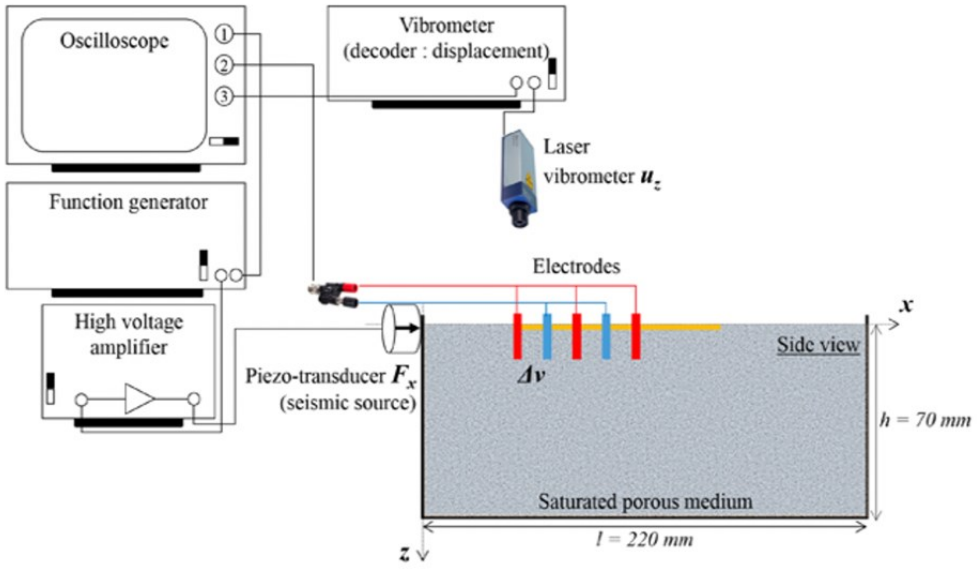

Figure 5: Schematic representation of SEE experiment (Devi et al., 2018). An acoustic wave generated by a piezoelectric transducer propagates within saturated sand in a box. Vertical electrodes buried in the sand measure the propagating coseismic SEE, while a laser interferometer (top) measures the seismic wave at the top of the sand.

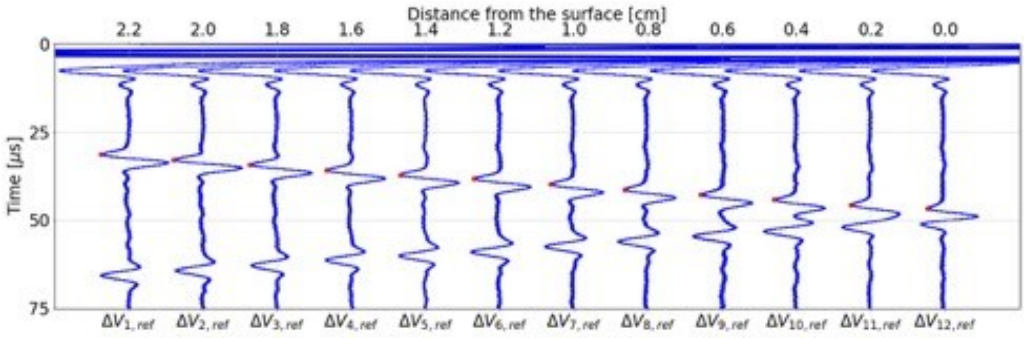

Figure 6: Coseismic electric signal recorded at electrodes buried in the sand.

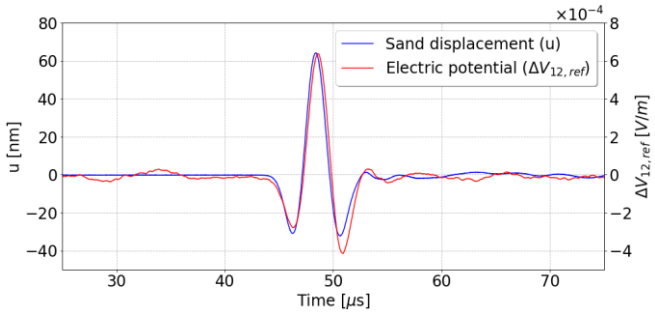

Figure 7: Direct comparison of the seismic displacement measured at the sand surface and coseismic electric signal.

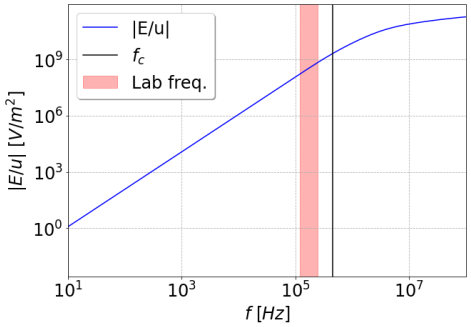

Figure 8: Theoretical transfer function for Granite sand.

4. FIELD EXPERIEMENTS

4.1 Svelvik CO_2 Field Lab

A field experiment was performed by NORCE to test seismoelectric acquisition at the Svelvik CO_2 Field Lab in September 2021. The Svelvik CO_2 Field Lab is an ECCSEL (European Research Infrastructure for CO_2 Capture, Utilisation, Transport and Storage) facility established in 2019 and is located at Svelvik, ~50 km South of Oslo (Figure 9). The geometry of the field deployment is illustrated on Figure 10. Figure 11 shows an example of raw SEE and seismic datasets recorded in well M2 and at the surface, respectively, when using a sparker in well M4 at 60 m depth. Further analysis is needed and will involve access to fiber dataset within well M2. This fiber dataset will allow us to directly compare collocated seismic data with the SEE signals to identify coseismic signals and isolate interface responses.

Figure 9: The CO_2 lab lies in a disused part of a sand quarry. The test site was funded by Norwegian and European grants and is operated by SINTEF (https://www.sintef.no/en/).

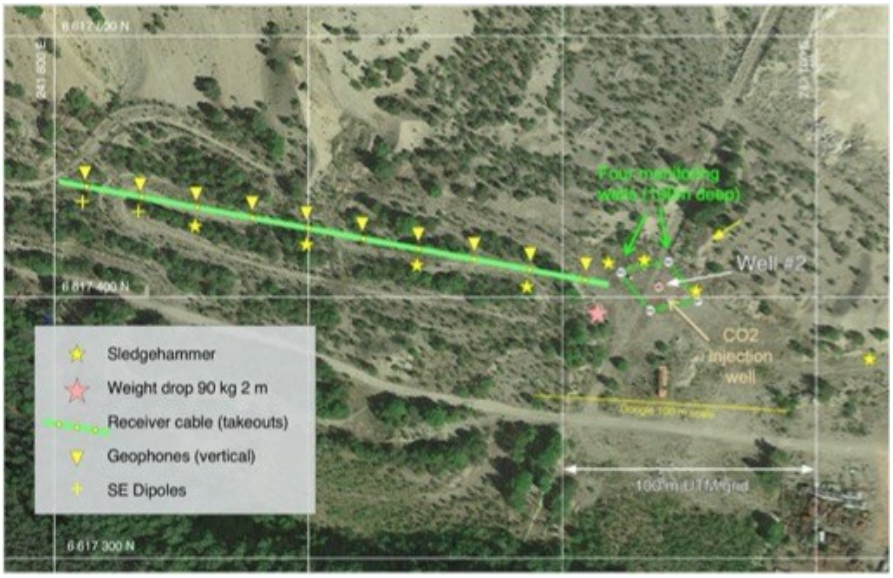

Figure 10: Geometry of the field deployment.

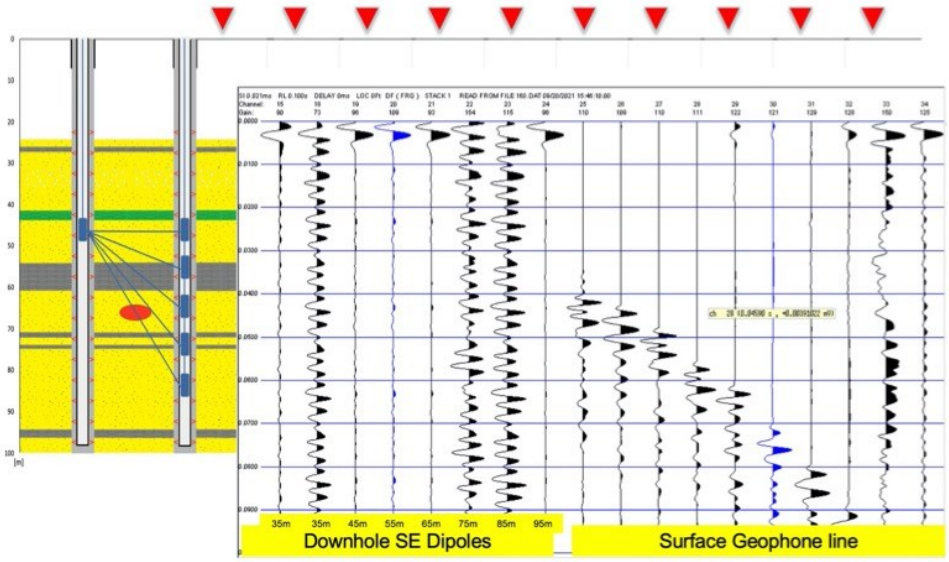

Figure 11: Downhole SEE and surface seismic datasets. Geometry of the acquisition is also shown in the background.

4.2 La Sioule-Miouze Geothermal Field Test

Next, to show the practical use of SEE for geothermal monitoring, we are planning a proof-of-concept field survey at a geothermal site located in France and operated by TLS Geothermics since 2017. Geothermal exploration analysis based on field surveys and modeling were carried out between 2015 and 2018 using geological, geochemical, and geophysical acquisitions using magnetotelluric, gravity, and passive seismic methods (Figure 12). This led to the identification of a favorable geothermal prospect hosted in a granitic fault zone. A deep drilling is planned in 2022 with a target at 3500 m depth. A shallow 200 m deep well will also be drilled close by and will carry SEE instrumentation. The approach is to use not only the potential local microseismicity as a source to the SEE signals but also the drill used during the deep drilling, which will act as a seismic source. Figure 13 shows a map view of the site with the position of the planned shallow well as well as a resistivity log, microseismicity, and faults structure.

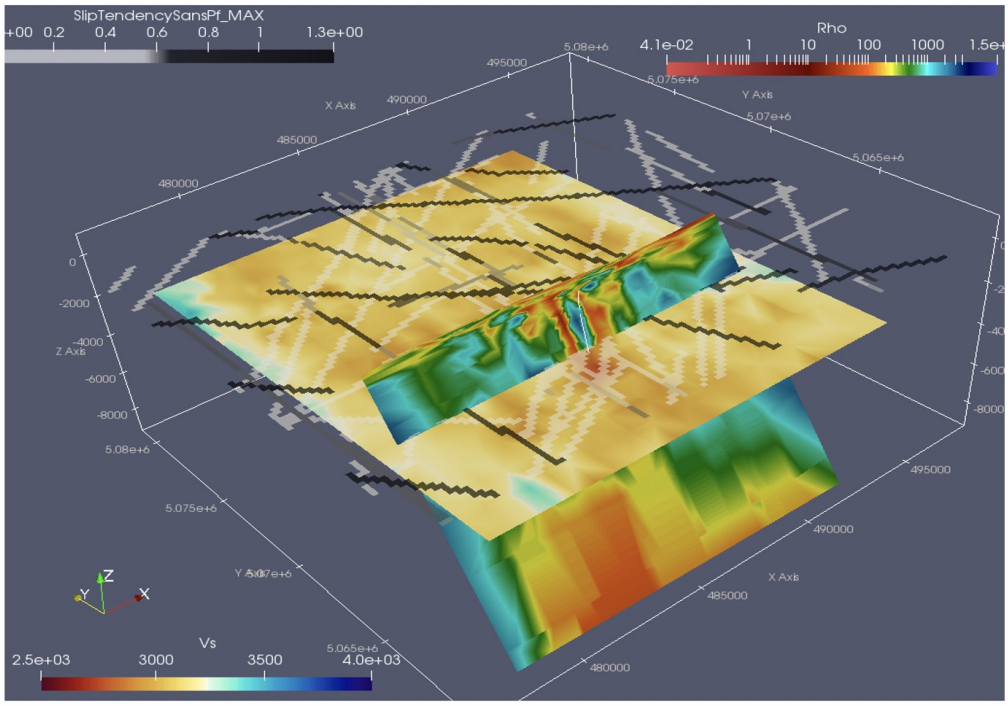

Figure 12: Illustration of the current state of knowledge of the Sioule-Miouze geothermal system from a structural (illustrated here with a possible slip tendency), electrical resistivity (Rho) and shear wave velocity (Vs) point of view. The expected deep drilling is illustrated by the white line. A shallow drilling will be located close to this deep drilling and carry SEE instrumentation.

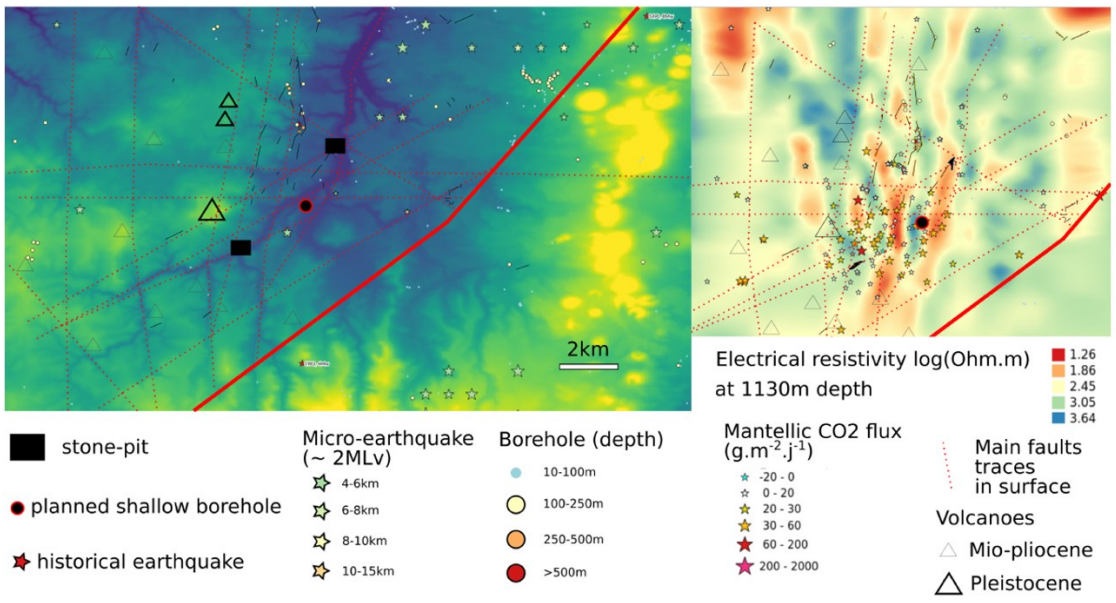

Figure 13: Map view of the Sioule-Miouze field test with microseismicity, main faults, and electrical resistivity.

5. CONCLUSION

We show a successful numerical implementation of seismic-to-electric conversion to model seismoelectric effects signals characterized by three types of signals in agreement with the theory, such as a coseismic electric signal, a quasi-instantaneous electric signal from seismic source, and a quasi-instantaneous interface response.

SEE sensitivity to geothermal environment can be tested experimentally and inform optimal field deployment. The field deployment planned in the Sioule-Miouze geothermal site will in addition allow the testing of several acoustic sources.

Preliminary SEE field acquisition at Svelvik CO2 Field Lab shows that SEE dataset can be collected, but further analysis needs to be performed to validate the presence of coseismic and interface responses. SEE interface response fields created at changes in properties can detect thin layers and other fine-scaled structural features such as fractures beyond the seismic resolution (e.g., Grobbe and Slob, 2016).

SEE technique can offer a more cost-effective approach necessitating only seismic sources and collocated geophones & antennas, compared to separate seismic & EM techniques necessitating two separate sources and deployments.

Finally, in this contribution we only focused on forward numerical modeling of SEE, understanding that it is the first step toward full inversion of SEE (seismic & electric) properties for monitoring and subsurface characterization. SEE dataset can capture unique information on geothermal reservoir properties and heterogeneities, such as resistivity, salinity, degree of saturation and viscosity, as opposed to purely seismic or purely EM records.

ACKNOWLEDGEMENTS

This project has been subsidized through the Cofund GEOTHERMICA by the U.S. Department of Energy, Office of Energy Efficiency and Renewable Energy, under Contract DE-AC52-07NA27344 with Lawrence Livermore National Laboratory, by the French Environment and Energy Management Agency and E2S UPPA, and by the Research Council of Norway. Svelvik CO_2 Field Lab test field experiment was made possible through collaborations with the DigiMon project, SINTEF, and Professor Karl E. Butler, University of New Brunswick, Canada. LLNL-PROC-830959.

REFERENCES

Barucq, H., J., Diaz, R.-C., Meyer, and H., Pham, 2021, Implementation of Hybridizable Discontinuous Galerkin method for time-harmonic anisotropic poroelasticity in two dimensions: International Journal for Numerical Methods in Engineering, 122: 3015–3043.

Biot, M. A., 1956a, Theory of propagation of elastic waves in a fluid saturated porous solid. I Low frequency range: Journal of the Acoustical Society of America, 28, 168-178.

Biot, M. A., 1956b, Theory of propagation of elastic waves in a fluid saturated porous solid. II Higher frequency range: Journal of the Acoustical Society of America, 28, 179-191.

Bordes, C., L. Jouniaux, M. Dietrich, J. P. Pozzi, and S. Garambois, 2006, First laboratory measurements of seismo-magnetic conversions in fluid-filled Fontainebleau sand: Geophysical Research Letters, 33, L01302, doi:10.1029/2005GL024582.

Bordes, C., L. Jouniaux, S. Garambois, M. Dietrich, J. P. Pozzi, and S. Gaffet, 2008, Evidence of the theoretically predicted seismo-magnetic conversion: Geophysical Journal International, 174, 489-504.

Devi, M.S., S. Garambois, D. Brito, M. Dietrich, V. Poydenot, and C. Bordes, 2018, A novel approach for seismoelectric measurements using multielectrode arrangements: II—Laboratory measurements: Geophysical Journal International, 214, 1783–1799.

Grobbe, N. and E. C. Slob, 2016, Seismo-electromagnetic thin-bed responses: Natural signal enhancements: Journal of Geophysical Research - Solid Earth, 121, 2460-2479.

Haines, S. S., 2004, Seismoelectric imaging of shallow targets: PhD Thesis, Stanford University.

Holzhauer, J., D. Brito, C. Bordes, Y. Brun, and B. Guatarbes, 2017, Experimental quantification of the seismoelectric transfer function and its dependence on conductivity and saturation in loose sand: Geophysical Prospecting, 65, 1097-1120.

Pride, S. R., 1994, Governing equations for the coupled electromagnetics and acoustics of porous media: Physical Review, B, 50, 15678–15696.

Morency, C., 2020, Electromagnetic wave propagation based upon spectral-element methodology in dispersive and attenuating media: Geophysical Journal International, 220, 951-966.

Morency, C., and J. Tromp, 2008, Spectral-element simulations of wave propagation in porous media, Geophysical Journal International, 175, 301-345.

Shen, C., D. Brito, J. Diaz, F. Sanjuan, C. Bordes, and S. Garambois, 2022, Pulsed-laser source characterization in laboratory seismic experiments. Geomech. Geophys. Geo-energ. Geo-resour. 8, 16.